small
NANO MICRO

Measuring True Young's Modulus of a Cantilevered Nanowire: Effect of Clamping on Resonance Frequency

*Qingquan Qin, Feng Xu, Yongqing Cao, Paul I. Ro, and Yong Zhu**

The effect of clamping on resonance frequency and thus measured Young's modulus of nanowires (NWs) is systematically investigated via a combined experimental and simulation approach. ZnO NWs are used in this work as an example. The resonance tests are performed in situ inside a scanning electron microscope and the NWs are cantilevered on a tungsten probe by electron-beam-induced deposition (EBID) of hydrocarbon. EBID is repeated several times to deposit more hydrocarbons at the same location. The resonance frequency increases with the increasing clamp size until approaching that under the "fixed" boundary condition. The critical clamp size is identified as a function of NW diameter and NW Young's modulus. This work: 1) exemplifies the importance of considering the effect of clamping in measurements of Young's modulus using the resonance method, and 2) demonstrates that the true Young's modulus can be measured if the critical clamp size is reached. Design guidelines on the critical clamp size are provided. Such design guidelines can be extended to other one-dimensional nanostructures such as carbon nanotubes.

1. Introduction

One-dimensional (1D) nanostructures such as nanowires (NWs) and nanotubes are critical building blocks of nanotechnologies.[1] They exhibit outstanding mechanical properties in addition to electrical, thermal and optical properties. As such, they have been demonstrated in a broad range of applications including nanosensors, nanoelectromechanical systems,[2] and nanoscale energy harvesting/storage.[3] It has been reported that size-dependent mechanical properties arise as the characteristic dimension approaches sub-100 nm.[4] Therefore, it is important to accurately measure their mechanical properties, which is key to gaining fundamental understanding of surface effects on such properties.

Mechanical testing of 1D nanostructures is challenging in spite of recent advances.[5] Notable experimental methods include vibration/resonance,[4b,6] bending,[7] tension,[8] and nanoindentation.[9] In the resonance test, amplitude and resonance frequency of NWs can be measured by microscopy imaging. Following a simple beam theory, Young's modulus of NWs can be calculated. The uncertainty in boundary condition could lead to considerable errors in the Young's modulus. In the bending method, atomic force microscopy (AFM) is used to deflect a single NW and measure the load and displacement simultaneously. However, the AFM tip might slip from the NW in the cantilevered (single-clamped) case while the induced axial force might cause a nonlinear effect that is typically not considered in data reduction in the double-clamped case. The uniaxial tensile test is the most straightforward method for mechanical characterization of bulk materials. Microelectromechanical systems (MEMS) have recently emerged as a promising tool for in situ electron microscopy tensile testing of NWs.[8b,10] However, the tensile testing of NWs generally requires specific nanomanipulation and testing procedures, which could be laborious.

Resonance is a simple and widely used method to measure Young's modulus of NWs. According to a simple beam theory, the nth mode resonance frequency of a single-clamped (cantilevered) beam is

$$f_n = \frac{\beta_n^2}{2\pi L^2}\sqrt{\frac{E I}{\rho A}} \quad (1)$$

Q. Qin,[+] F. Xu,[+] Dr. Y. Cao, Prof. P. I. Ro, Prof. Y. Zhu
Department of Mechanical and Aerospace Engineering
North Carolina State University
Raleigh, North Carolina 27695-7910, USA
E-mail: yong_zhu@ncsu.edu
[+] These authors contributed equally to this work

DOI: 10.1002/smll.201200314

where E is the Young's modulus, I is the moment of inertia, L is the beam length, A is the cross-sectional area and ρ is the beam density. The β_n term is the eigenvalue from the characteristic equation: $\cos\beta_n \sin\beta_n + 1 = 0$; $\beta_0 = 1.875$, $\beta_1 = 4.694$, and $\beta_2 = 7.855$ correspond to the first three resonance modes for any cantilevered beam.[11] When the resonance frequency is measured, the Young's modulus can be calculated according to Equation (1). However, Equation (1) assumes the "fixed" boundary condition that requires zero displacement and slope at the "fixed" end. For NW testing, two methods are often used to attach NWs to a substrate. The first method is to grow NWs on top of a substrate.[4b] In this case, it is reasonable to assume a "fixed" boundary condition. But this method is limited to those NWs that can be directly grown on the substrate; plus, such type of NW growth is not trivial. The second method involves picking up a single NW (e.g., using a nanomanipulator), attaching it to a substrate and clamping it. One way for clamping a NW is electron-beam-induced deposition (EBID) of residual hydrocarbon in a scanning electron microscope (SEM) chamber or intentionally introduced precursor gas. This method is general and can be applied to any NWs. However, the clamping materials are compliant, which leads to a concern whether the boundary condition can be assumed "fixed".

In this paper, we systematically investigate the effect of clamping on the resonance frequency and thus the Young's modulus of ZnO NWs. The reason to study ZnO NWs is that they are one of the most important functional NWs[12] and their mechanical properties have been relatively well understood.[4a,b,e] In situ mechanical resonance tests of ZnO NWs were performed inside a SEM, where the NWs were clamped on a tungsten probe by EBID of hydrocarbon (available in the SEM chamber). EBID was repeated several times to deposit more clamping material on the same location; after each deposition the resonance frequency was measured. The resonance frequency increased with the clamp size initially but then gradually approached a constant value. Finite element analysis was carried out to simulate the effect of the clamp size on the NW resonance frequency, which agreed well with the experimental results. Both experiments and simulations showed that with sufficient clamp material, the resonance frequency converges to that under the "fixed' boundary condition (i.e., the "fixed" boundary condition is met).

2. Results and Discussion

Figure 1a shows a schematic of the experimental setup. A piezoelectric sheet was used to provide mechanical vibration. The piezoelectric sheet was glued to the SEM sample holder on one side and a tungsten probe was glued to the other side. NWs were later clamped on the tungsten probe for vibration tests. The ZnO NWs used in this work were uniform in diameter along the growth direction. Figure 1b shows a stationary ZnO NW with one end clamped on the tip of the first tungsten probe as mentioned above. Figure 1c shows the vibrated NW under resonance. The NWs were only vibrated at the fundamental harmonic mode.

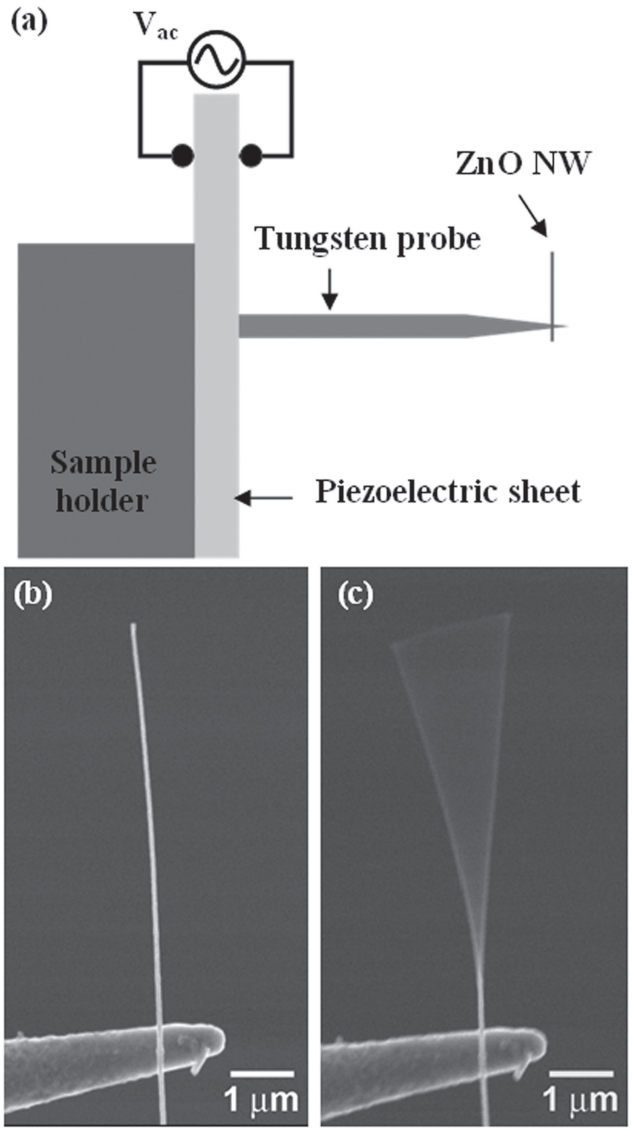

Figure 1. a) Schematic of the experimental setup. b) SEM image of a stationary ZnO NW with one end clamped on the tip of the tungsten probe. c) SEM image of the ZnO NW under resonance at the fundamental harmonic mode.

The procedure to test the effect of clamping on the resonance frequency of ZnO NWs was as follows. First, SEM images around the resonance frequency of the initially clamped NW were taken (the resonance frequency was determined later). EBID was then used again to deposit more carbonaceous material at the same clamp location. SEM images around the new resonance frequency were taken again. The process of depositing more material at the same clamp location and taking SEM images around the new resonance frequency was repeated several times.

Figure 2a shows the amplitude–frequency characteristics of a NW after each deposition. Overall, five deposition times were used for this NW. The deposition line widths were 19, 25, 39, 65, and 79 nm, respectively. It can be seen that the resonance frequency increased after each additional deposition, but approached a constant value after the line width of 65 nm

small 2012,
DOI: 10.1002/smll.201200314

small NANO MICRO

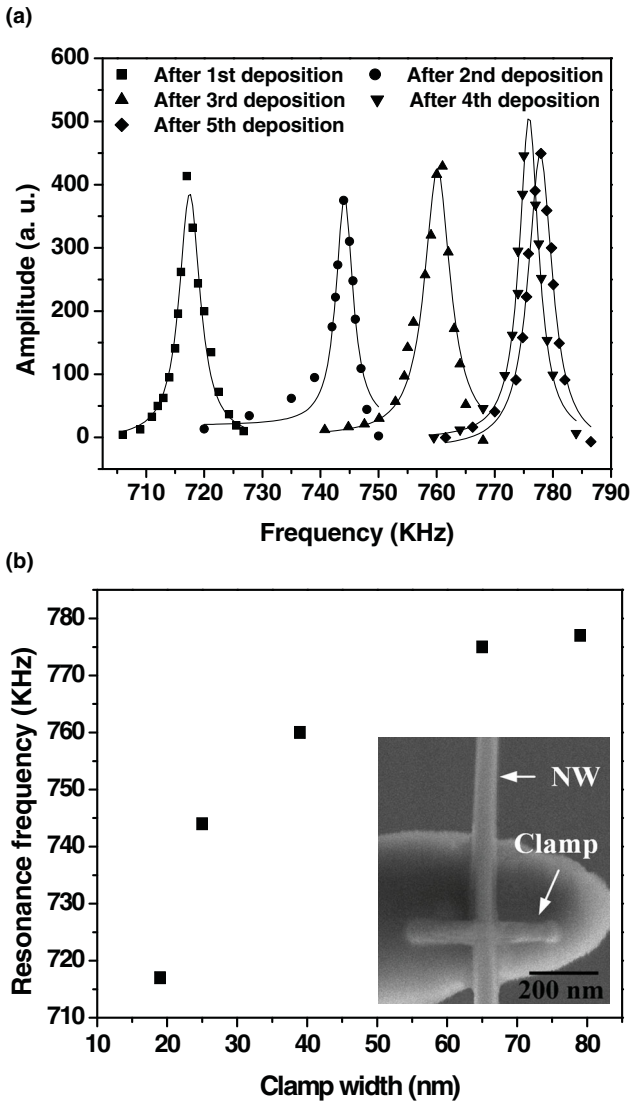

Figure 2. a) The amplitude–frequency characteristics of a NW after each deposition. The curves show the Lorentzian fits. b) The resonance frequency of the NW as a function of the clamp width. The inset shows SEM image of the NW clamped by a line pattern (deposited by EBID).

(Figure 2b). SEM image in the inset of Figure 2b shows a representative line pattern of hydrocarbon (deposited by EBID). The length of the deposition (clamp) line was measured to be ~440 nm, which was kept the same in spite of changing the width. The line width increased after each deposition. The line width was measured from SEM images, but not the line thickness. To systematically characterize the dimensions of the deposition lines, hydrocarbon was deposited on a polished tungsten foil (similar to the tungsten probe). On the tungsten foil, SEM and AFM (Park Systems, XE-70) characterization can be conducted to measure the width and thickness of the same deposition line, respectively (see Supporting Information (SI)). The line thickness was found to increase with the line width; their relationship is shown in Figure S1d of the SI.

Finite element analysis (ABAQUS) was used to simulate the effect of deposition (clamp) on the resonance

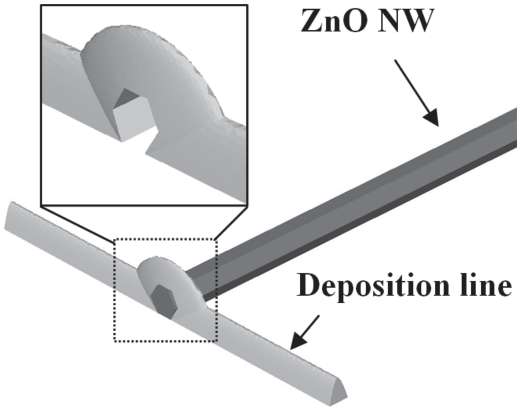

Figure 3. 3D view of the configuration used in the simulation including the deposition line and the ZnO NW. The inset shows a magnified view of the middle part of the deposition line.

frequency. **Figure 3** shows the configuration used in the simulation including the deposition line and the ZnO NW. Fixed boundary condition was applied to the bottom of the deposition line, and the NW was tied to the deposition line. 20-node quadratic brick elements (C3D20R) and 4-node linear tetrahedron elements (C3D4) were used for the NW and the deposition line, respectively. A numerical method, so-called linear perturbation step, available in ABAQUS was used to extract the resonance frequencies. The dimensions of the deposition line used here were obtained from Figure S1d of the SI; the range of the line width was set to be from 10 to 83 nm while the corresponding thickness ranged from 28 to 117 nm. The cross section of the deposition line was a parabolic shape (Figure 3c), which was found to best fit the experimental results when compared to other shapes such as semicircle/rectangle and rectangle (see SI). The length of the deposition line was set to be 440 nm, the same as that in the experiments. The Young's modulus of the deposited material was 40 GPa.[13] The dimension of each NW was measured from experiments. The Young's modulus of ZnO NWs has been found to depend on the NW diameter and loading mode (i.e., tension versus bending).[4e,14] The Young's moduli of NWs used in the simulation were taken from those under the same loading mode (i.e., resonance tests with NWs directly grown on a substrate).[4b]

Three NWs were tested in our experiments and each NW underwent multiple depositions. The dimensions of these NWs are listed in **Table 1**. The length of each NW was measured from the middle of the deposition line to the vibrating end of the NW. The Young's moduli of the NWs corresponding to their diameters are also listed in the Table 1 (extrapolated from reference[4b]). Using these values in the

Table 1. The dimensions of the NWs and the extrapolated Young's moduli of the NWs corresponding to their diameters.

	NW1	NW2	NW3
Diameter [nm]	55	60	62
Length [μm]	7.14	7.04	6.73
Young's modulus [GPa]	173	168	167

DOI: 10.1002/smll.201200314

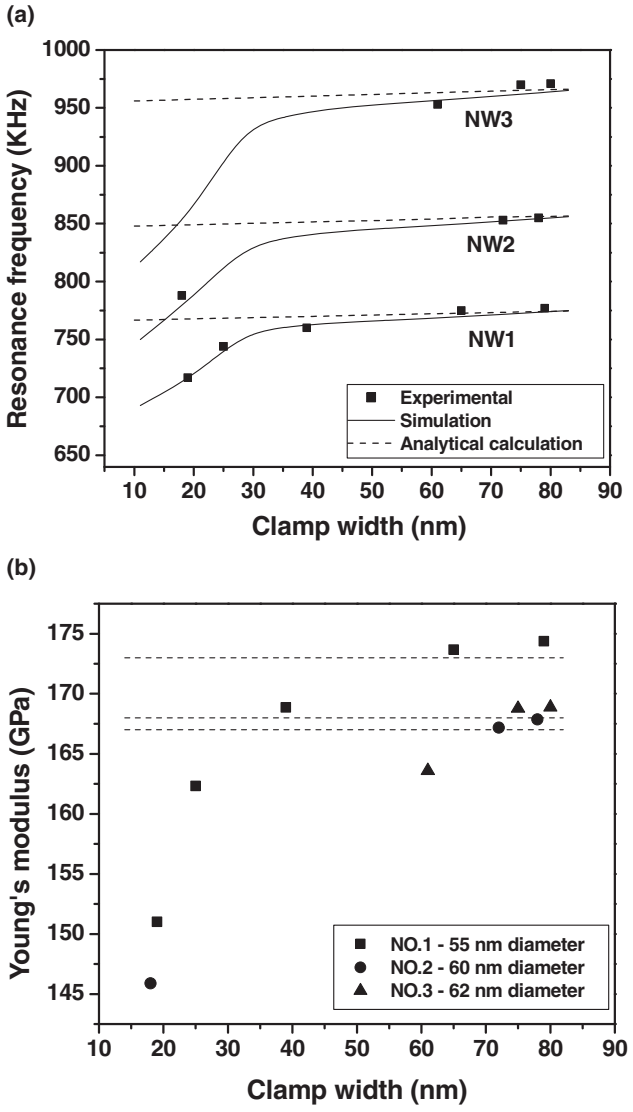

Figure 4. a) Plots of the resonance frequencies of the three NWs versus clamp widths from the experiments, simulation and analytical calculation. In the analytical solution, since the effective NW length decreases with increasing clamp width, the resonance frequency increase slightly. b) Young's moduli of the three NWs as a function the clamp width, as calculated from the experimental resonance frequencies using the beam theory. The dash lines indicate the Young's moduli of the NWs under "fixed" boundary condition.

simulation, the resonance frequencies of these NWs with different clamp widths (and thus different thicknesses) were obtained. Both experimental and simulation results are summarized and plotted in **Figure 4**a, showing good agreement. The resonance frequency increased rapidly with the clamp width in the beginning and gradually approached a constant value.

However, the key question is not yet answered: is it acceptable to treat a clamped NW as the "fixed" boundary condition? To answer this question, we calculate the resonance frequencies with the Young's moduli and our measured dimensions assuming the "fixed" boundary condition (i.e., Equation (1)), and compare them with the experimental and simulation results. ZnO NWs have hexagonal cross sections, so the resonance frequency at the fundamental harmonic mode can be written as

$$f_0 = \frac{\beta_0^2}{2\pi}\frac{D}{L^2}\sqrt{\frac{5E}{96\rho}} \quad (2)$$

where D is the beam diameter (distance between two diametrically opposite vertices for a hexagon). The analytical results are also plotted in Figure 4a as dashed lines. Note that the slight change in the resonance frequency is a result of the change in effective NW length (due to the increase in clamp width). The effective NW length (defined as the length from the closer edge of the deposition line to the free end of the NW) is used in the analytical calculation. Apparently, with the increase of clamp size, the discrepancy between the analytical calculation and experiment/simulation decreases. Especially when the clamp width approaches 80 nm, the resonance frequencies from experiments and simulations are almost identical to that from the analytical calculation. Thus, it is reasonable to conclude that the "fixed" boundary condition is met when the clamp width reaches 80 nm or larger, for the ZnO NWs tested in this work (diameters between 55 and 62 nm).

Figure 4b plots the measured Young's moduli of the three NWs as a function the clamp width, as calculated from the measured resonance frequencies using Equation (2). Note that the effective NW lengths are used in the calculation. For all the NWs, the Young's moduli increase with the clamp size and approach the reported values.[4b] This indicates that the errors in the Young's modulus measurement from the resonance test can be minimized by increasing the deposition width. Two additional remarks are noted. First, when the clamp size is small, the resultant error in Young's modulus can be as large as 13.4% (for instance, for NW1). The above analysis provides a rationale behind the low modulus values reported for ZnO nanobelts and NWs (also using the resonance test).[15] Among other reasons, the low values might be caused by the imperfect boundary conditions, in which the nanostructures were barely attached to a gold ball or tungsten probe without deposition clamping. Second, the change in effective NW length causes a slight variation in the calculated resonance frequency (as shown in dashed lines in Figure 4a) and thus Young's modulus. However, the change in effective NW length is very small (40 nm versus a typical NW length of over 6 μm). According to Equation (2), the relative error is less than 2.6% for a measured resonance frequency, which might be negligible for most applications.

To provide a design guideline for those who might use the EBID of hydrocarbon for clamping NWs, a parametric study was further pursued to illustrate the effects of clamp length, NW diameter and NW Young's modulus. The clamp length does not play an important role as long as it exceeds about 4 times of the NW diameter, as shown in Figure S3 of the SI. But the NW diameter and NW Young's modulus play important roles, thus imposing stringent requirement on the clamp width to achieve the "fixed" boundary condition. **Figure 5** shows the effect of the NW diameter on the resonance frequency (with a constant NW Young's modulus of 168 GPa).

DOI: 10.1002/smll.201200314

NANO MICRO small

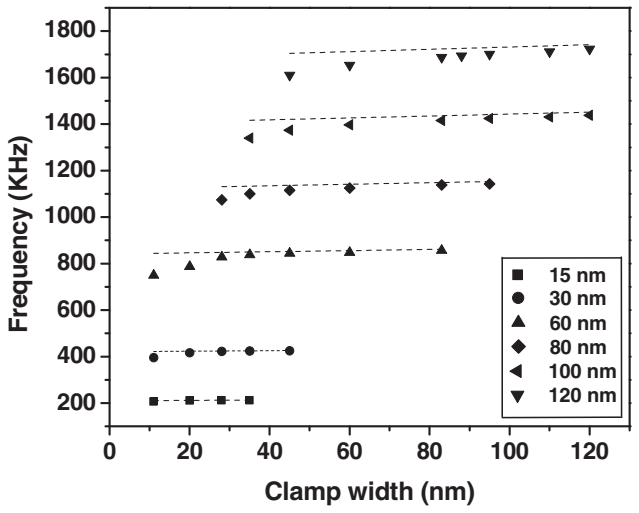

Figure 5. Resonance frequency as a function of clamp width for NWs with different diameters (from 15 nm to 120 nm). A constant NW Young's modulus (168 GPa) is used here. The dash lines indicate the resonance frequencies under "fixed" boundary condition.

More details can be seen in Figure S4 of the SI. For each NW diameter, the NW resonance frequency increases with the clamp width. The critical clamp width, above which the "fixed" boundary condition is reached, appears to be approximately equal to the NW diameter. **Figure 6** shows the effect of the NW Young's modulus on the resonance frequency (with a constant NW diameter of 60 nm). For each Young's modulus, the resonance frequency increases with the clamp width. The critical clamp width appears to increase linearly with the resonance frequency under the "fixed" boundary condition (i.e., square root of the NW Young's modulus according to Equation (1)). Note that the critical width is defined as the width when the difference between the calculated (dashed line) and simulated (dots) resonance frequency of a NW is less than

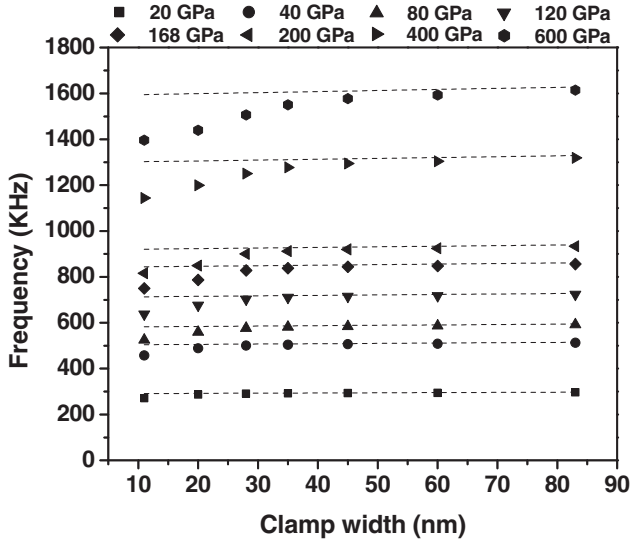

Figure 6. Resonance frequency as a function of clamp width for NWs with different Young's modulus (from 20 GPa to 600 GPa). A constant NW diameter (60 nm) is used here. The dash lines indicate the resonance frequencies under "fixed" boundary condition.

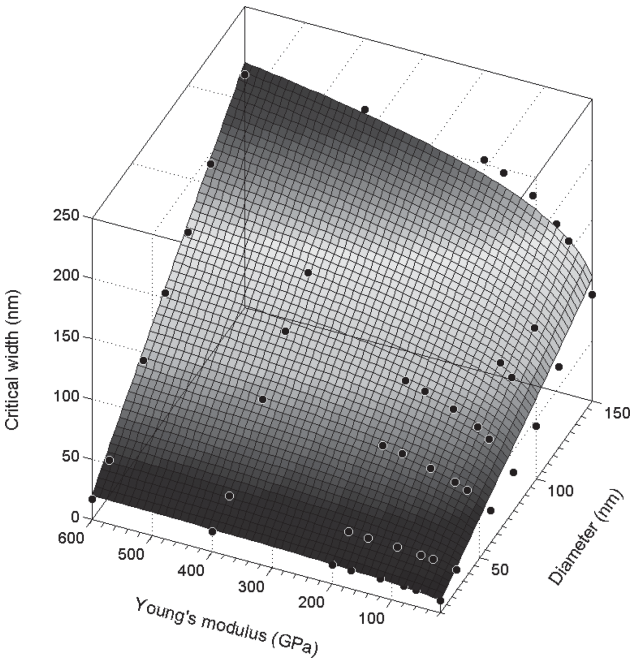

Figure 7. The critical clamp width as functions of diameter and Young's modulus of NW. The fitting plane shows $w_{cr} = \alpha D(E/E_{hc})^n$, with $\alpha = 0.786$ and $n = 0.2$.

1% in Figure 5. It is of additional note that the aspect ratio of NW (NW length over diameter) does not play an important role in determining critical clamp width as long as the ratio is larger than 40, as shown in Figure S5 of the SI.

It becomes clear that the critical clamp width depends on the NW diameter and the NW Young's modulus. **Figure 7** plots the critical clamp width as a function of the NW diameter and the NW Young's modulus. A plane fitting was applied to the data, and a simple scaling law was extracted from Figure 7, viz.,

$$w_{cr} = \alpha D \left(\frac{E}{E_{hc}} \right)^n \tag{3}$$

where w_{cr} is the critical clamp width, D is the NW diameter, E is the NW Young's modulus, E_{hc} is the hydrocarbon Young's modulus (= 40 GPa[13]), α is a constant (= 0.786 in this work) and n equal to 0.2. The coefficient of determination (R^2) using this fitting function is 0.97, indicating that the function fits the data very well.

3. Conclusion

We have systematically investigated the effect of clamping on the resonance frequency and hence the measured Young's modulus of cantilevered NWs by a combined experiment and simulation approach. The resonance tests were performed in situ inside a SEM with ZnO NWs clamped on tungsten probes by EBID of hydrocarbon. EBID was repeated several times to deposit more hydrocarbons at the same location and the resonance frequencies were measured after each deposition until a stable resonance frequency was

DOI: 10.1002/smll.201200314

obtained. Finite element analysis was carried out to simulate the clamping effect, which agreed well with the experimental results. Initially the resonance frequency increased rapidly with the clamp size. When the clamp width reached a critical value, the resonance frequency approached that under the "fixed' boundary condition. Further numerical simulations were performed to investigate the effect of NW diameter and Young's modulus on the clamp size (including width and length), which led to a simple scaling law that can be used as guidelines for future designs. Our work demonstrates that true Young's modulus can be measured if the critical clamp size is reached. Also in calculating the Young's modulus, it is acceptable to use the nominal NW length (from the center of the clamp to the vibrating end of the NW) instead of the effective NW length (from the closer edge of the deposition line to the vibrating end of the NW). Our work provides design guidelines on the critical clamp size, which is useful in accurate measurement of the Young's modulus of 1D nanostructures using the resonance method.

4. Experimental Section

The ZnO NWs were synthesized by the vapor–liquid–solid method on Si/SiO_2 substrates with Au colloids as the catalysts.[16] The mechanical resonance tests were performed inside an SEM (JEOL 6400F). A nanomanipulator (Klocke Nanotechnik, Germany) with 1 nm resolution and 1 cm travel range in three orthogonal directions was used to pick up protruding NWs from the Si substrate following the procedure outlined by Zhu and Espinosa.[8b] After a ZnO NW was clamped to the second tungsten probe on the nanomanipulator using EBID of carbonaceous materials in the SEM chamber, the NW was pulled away from the Si substrate, moved toward the first tungsten probe (glued to the piezoelectric sheet). Using EBID again, the NW was clamped on the tip of the first probe, and then the other clamp was broken off. This depends on the strength difference of the two clamps; the clamp on the second probe is intentionally weaker than that on the first probe. The strength difference was achieved by controlling the deposition time. Note that the second probe broke off from the short end of the NW (Figure 1a). Subsequently, the piezoelectric sheet was excited into mechanical vibration by applying an AC voltage of 0.5 V, which drove mechanical resonance in the attached NW (through the first probe). For mechanically induced resonance of NWs, the frequency of the applied AC signal is the NW's resonance frequency. The case of electrically induced resonance could be more complicated.[11] Around the resonance frequency of each NW, SEM images of the vibrating NW were taken at a number of frequencies, from which the vibration amplitude was measured as a function of the frequency (Figure 2a). Then the resonance frequency can be determined from the amplitude-frequency plot.

Supporting Information

Supporting Information is available from the Wiley Online Library or from the author.

Acknowledgements

This work was supported by the National Science Foundation under Award Nos. CMMI-1030637 and CMMI-1129817. The authors thank Prof. Y. Gu for providing the ZnO NW samples and Prof. X. Jiang for providing the piezoelectric sheet.

[1] a) R. H. Baughman, A. A. Zakhidov, W. A. de Heer, *Science* **2002**, *297*, 787; b) W. Lu, C. M. Lieber, *J. Phys. D: Appl. Phys.* **2006**, *39*, R387.
[2] X. L. Feng, R. R. He, P. D. Yang, M. L. Roukes, *Nano Lett.* **2007**, *7*, 1953.
[3] a) Z. L. Wang, J. H. Song, *Science* **2006**, *312*, 242; b) C. K. Chan, H. L. Peng, G. Liu, K. McIlwrath, X. F. Zhang, R. A. Huggins, Y. Cui, *Nat. Nanotechnol.* **2008**, *3*, 31.
[4] a) F. Xu, Q. Q. Qin, A. Mishra, Y. Gu, Y. Zhu, *Nano Res.* **2010**, *3*, 271; b) C. Q. Chen, Y. Shi, Y. S. Zhang, J. Zhu, Y. J. Yan, *Phys. Rev. Lett.* **2006**, *96*, 075505; c) Y. Zhu, F. Xu, Q. Q. Qin, W. Y. Fung, W. Lu, *Nano Lett.* **2009**, *9*, 3934; d) H. S. Park, W. Cai, H. D. Espinosa, H. C. Huang, *MRS Bull* **2009**, *34*, 178; e) R. Agrawal, B. Peng,E. E. Gdoutos, H. D. Espinosa, *Nano Lett.* **2008**, *8*, 3668.
[5] Y. Zhu, C. Ke, H. D. Espinosa, *Exp. Mech.* **2007**, *47*, 7.
[6] P. Poncharal, Z. L. Wang, D. Ugarte, W. A. de Heer, *Science* **1999**, *283*, 1513.
[7] a) E. W. Wong, P. E. Sheehan, C. M. Lieber, *Science* **1997**, *277*, 1971–1975; b) B. Wu, A. Heidelberg, J. J. Boland, *Nat. Mater.* **2005**, *4*, 525.
[8] a) M. F. Yu, O. Lourie, M. J. Dyer, K. Moloni, T. F. Kelly, R. S. Ruoff, *Science* **2000**, *287*, 637; b) Y. Zhu, H. D. Espinosa, *Proc. Natl. Acad. Sci. USA* **2005**, *102*, 14503.
[9] X. D. Li, H. S. Gao, C. J. Murphy, K. K. Caswell, *Nano Lett.* **2003**, *3*, 1495.
[10] a) Y. Zhu, N. Moldovan, H. D. Espinosa, *Appl. Phys. Lett.* **2005**, *86*, 013506; b) A. V. Desai, M. A. Haque, *Sens. Actuators, A* **2007**, *134*, 169.
[11] W. Q. Ding, L. Calabri, X. Q. Chen, K. M. Kohhaas, R. S. Ruoff, *Compos. Sci. Technol.* **2006**, *66*, 1112.
[12] Z. L. Wang, *J. Phys.: Condens. Matter* **2004**, *16*, R829.
[13] W. Ding, D. A. Dikin, X. Chen, R. D. Piner, R. S. Ruoff, E. Zussman, X. Wang, X. Li, *J. Appl. Phys.* **2005**, *98*, 014905.
[14] M. R. He, Y. Shi, W. Zhou, J. W. Chen, Y. J. Yan, J. Zhu, *Appl Phys Lett* **2009**, *95*, 091912.
[15] a) X. D. Bai, P. X. Gao, Z. L. Wang, E. G. Wang, *Appl. Phys. Lett.* **2003**, *82*, 4806; b) Y. H. Huang, X. D. Bai, Y. Zhang, *J. Phys.: Condens. Matter* **2006**, *18*, L179.
[16] A. Soudi, E. H. Khan, J. T. Dickinson, Y. Gu, *Nano Lett.* **2009**, *9*, 1844.

Received: February 10, 2012
Published online:

DOI: 10.1002/smll.201200314